

Quantum chaos associated with emergent event horizon in transition layer between type-I and type-II Weyl semimetals

Yu-Ge Chen^{1,2,3,*}, Xi Luo^{4,*}, Fei-Ye Li^{1,2,3}, Bin Chen⁴, and Yue Yu^{1,2,3}

1. State Key Laboratory of Surface Physics, Fudan University, Shanghai 200433, China

2. Center for Field Theory and Particle Physics, Department of Physics, Fudan University, Shanghai 200433, China

3. Collaborative Innovation Center of Advanced Microstructures, Nanjing 210093, China

4. College of Science, University of Shanghai for Science and Technology, Shanghai 200093, PR China

(Dated: March 27, 2019)

We present pairwise emergent event horizons in a transition layer between type-I and type-II Weyl semimetals (WSMs). The Hawking temperature defined by a novel surface gravity at the horizon may be as high as several tens of Kelvin. On the type-II WSM side, i.e., inside the horizons, the motion of the quasiparticles may be chaotic after a critical surface where they are governed by an effective inverted oscillator potential induced by the mismatching of the positions between the type-I and type-II nodes. In a relevant lattice model, we calculate out of time ordered correlators (OTOCs) of the quasiparticles. Inside the horizons, the OTOCs may fast scramble with a quantum Lyapunov exponent, which confirms the quantum chaotic behavior. After the Ehrenfest time, the scrambling is saturated as expected. Additionally, we see an extra quantum chaos in the lattice model which can not be described by the effective theory at the Weyl nodes.

Introductions. Recent developments on the frontier of theoretical physics research have entangled the black hole horizon physics with quantum chaos [1–7].

In condensed matter systems, the black hole analog had been pioneered by Unruh in transsonic fluid flow [8]. A quantum analog had been provided in Bose-Einstein condensation [9], and a magnonic black hole was predicted [10]. The exotic emergent geometries (or gravities) have also been studied in Fermi surface [11], fractional quantum Hall effects [12–15], graphene [16], deformed crystal [17], type-II Weyl semimetal (WSM) [18–21], and type-III Dirac semimetal [22]. Several systems may simulate the Hawking evaporation at a black hole event horizon [23, 24]. However, the chaotic behaviors at the horizon do not appear easily. For instance, for the trajectory of a moving particle outside of the horizon to be chaotic classically, there must be an external potential near the horizon [25]. The Lyapunov exponent is subject to a maximal chaotic bound, the surface gravity [1]. This bound is saturated for theories with AdS/CFT duality, such as the case in the Sachdev-Ye-Kitaev model [2–4].

Volovik et al recently studied the emergent metric in the inhomogeneous WSM [18–20]. They found a general correspondence between the emergent vielbein e_μ^i and the effective Hamiltonian near a Weyl node $\mathbf{K} = (K_x, K_y, K_z)$, i.e.,

$$H(\vec{q}) = e_\mu^i q_i \sigma^\mu, \quad (1)$$

where $\mu = 0, i$ with $i = x, y, z$; $q_i = k_i - K_i$; and $\sigma^\mu = (I, \sigma^i)$ are the identity and Pauli matrices. Here the Einstein's summation convention for repeated indices is used. The 'speed of light' v_F (the Fermi velocity), the electron band mass m_b , and \hbar are set to be unity unless

they are explicitly restored. The spectrum is given by

$$E(Q_i)_\pm = e_0^j [e^{-1}]_j^i Q_i \pm |\mathbf{Q}|. \quad (2)$$

where the vector $Q_i \equiv e_i^j q_j$. The vielbein components e_μ^i together with $e_0^0 = -1$ and $e_i^0 = 0$ define an emergent metric $g^{\mu\nu} = \eta^{\alpha\beta} e_\alpha^\mu e_\beta^\nu$ with the signature $\eta^{\mu\nu} = \text{diag}(-1, 1, 1, 1)$ [18]. The event horizon of this emergent geometry is determined by $|\mathbf{v}| = 1$ where $v^i = e_0^j [e^{-1}]_j^i$. A Weyl node is of type-I (type-II) if $|\mathbf{v}| < 1$ ($|\mathbf{v}| > 1$). Although the Weyl nodes with opposite chirality must emerge in pairs, the type of each node can be arbitrary [26, 27]. Volovik uses the Painlevé-Gullstrand metric which is spherically symmetric to study inhomogeneous WSM [19]. However, such a geometry is difficult to be realized in condensed matter materials.

Both type-I and type-II WSMs have been proposed and found [28–34]. In order to simulate an event horizon in a realizable geometry and study the chaos phenomena, we consider a type-I/type-II WSM transition layer where the type-I and type-II Weyl nodes nearly match (See Fig. 1(a)). Within the transition layer, a black/white hole planar horizon emerges effectively at a given plane in the transition layer where $|\mathbf{v}| = 1$. That is, the interpolation between the type-I and type-II WSM Hamiltonians. induces a columnar surface gravity. A fermionic shock wave and the Hawking evaporation are possible to be detected because the Hawking temperature may be as high as several tens of Kelvin.

In the effective Hamiltonian approach, we further find that when the Weyl nodes of the type-I and type-II do not completely match, the transition layer states inside and outside the horizon may be totally different: On the type-I WSM side, the transition layer state is described by the Landau levels of the WSM in an effective magnetic field. On the type-II side, after a characteristic plane, the transition layer state is governed by an effective inverted oscillator potential [35]. The latter is an intrinsic quan-

*These two authors contribute equally.

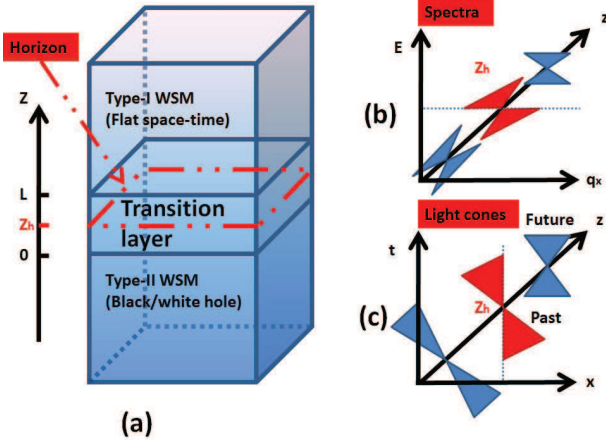


FIG. 1: (color online) (a) The transition layer between Type-I and Type-II WSMs. The critical surface $z = z_h$ serves as the horizon. (b) The spectra outside of, at and inside of the horizon, corresponding to type-I, critical and type-II WSM's. (c) The light cones outside of, at and inside of the horizon. In (b) and (c), we take $\alpha_z(z) = 0$ and project to the x -direction for simplicity.

tum open system in which there is quantum chaos [36].

In order to verify the quantum chaotic motion of the quasiparticles in the transition layer, we study a lattice model which reduces to the effective chaotic model in the transition layer in the long wave length limit. We calculate out of time ordered correlators (OTOCs) of the quasiparticles which characterize the quantum chaotic behavior [1–7, 37]. For a proper hopping strength in the transition layer with a sufficient layer thickness, we find that for quasiparticles inside inside the horizon, the OTOC shows a fast scrambling over a very short time and a quantum Lyapunov exponent is obtained. The OTOC also saturates after the Ehrenfest time. These two properties of OTOC indicates the existence of quantum chaos inside the horizon [38]. Meanwhile, in the OTOCs for the quasiparticles in the bulk of the WSM or the outside of the horizon in the transition layer, such fast scrambling does not appear and thus no evidence for the chaotic motion is found. Furthermore, the OTOCs in the lattice model exhibit another kind of quantum chaotic states which do not have the counterpart in the effective Hamiltonian approach.

Low energy effective model for transition layer. We consider that type-I and type-II WSMs couple as shown in Fig.1(a). The transition layer is located between $z = 0$ and $z = L$. Assuming \mathbf{K}^I (\mathbf{K}^{II}) is a Weyl node of the type-I (type-II) WSM in the regime $z > L$ ($z < 0$), and $|\mathbf{K}^I - \mathbf{K}^{II}| \ll K_0$ where K_0 is the distance between a pair of Weyl nodes in the bulk. The corresponding low energy effective Hamiltonian in the bulk of the type-I/II WSM is given by

$$H_{I/II} = (k_i - K_i^{I/II})\sigma^i - \alpha_{x,I/II}(k_x - K_x^{I/II}) - \alpha_{z,I/II}((k_z - K_z^{I/II})), \quad (3)$$

where $\alpha_{I/II} = (\alpha_{x,I/II}, 0, \alpha_{z,I/II})$ are parameters that tilt the Dirac cones. For the type-I WSM, $|\alpha_I| = \sqrt{\alpha_{xI}^2 + \alpha_{zI}^2} < 1$ and $|\alpha_{II}| = \sqrt{\alpha_{xII}^2 + \alpha_{zII}^2} > 1$ for the type-II WSM. We further assume $|\Delta\alpha| = |\alpha_{II} - \alpha_I| \ll 1$. The transition layer effective Hamiltonian can be approximated by a linear interpolation between H_I and H_{II} [39]

$$H(z) = H_{II} + (H_I - H_{II})\frac{z}{L}, \quad (4)$$

where $0 \leq z \leq L$. Defining $\mathbf{q} = \mathbf{k} - \mathbf{K}^{II}$ and $B_i = \frac{K_i^I - K_i^{II}}{L} = \frac{\Delta K_i}{L}$,

$$H(z) = (q_x + B_x z)\sigma^x + (q_y + B_y z)\sigma^y + (-i\partial_z + B_z z)\sigma^z - \alpha_x(z)(q_x + B_x z) - \alpha_z(z)(-i\partial_z + B_z z) + \dots \quad (5)$$

where “...” are high order terms including $O(\Delta\mathbf{K} \cdot \Delta\alpha)$ etc. q_z is replaced by $-i\partial_z$ and $B_x(B_y)$ can be thought as an effective magnetic field in the $y(x)$ -direction. One can perform a gauge transformation to change $-i\partial_z + B_z z$ to $-i\partial_z$ if the wave function ψ changes to $e^{-i\frac{B_z z^2}{2}}\psi$ accordingly. $\alpha(z)$ is a linear interpolation like $H(z)$

$$\alpha(z) = \alpha_{II} - \Delta\alpha\frac{z}{L}. \quad (6)$$

Since $|\Delta\alpha| \ll 1$, $\alpha(z)$ is a slow varying vector function of z . $|\alpha(z_h)| = 1$ determines the critical surface with $z = z_h$ which separates the type-I and type-II WSM, where

$$\frac{z_h}{L} = \frac{\Delta\alpha \cdot \alpha_{II} - \sqrt{(\Delta\alpha \cdot \alpha_{II})^2 - (\Delta\alpha)^2(\alpha_{II}^2 - 1)}}{(\Delta\alpha)^2} \quad (7)$$

Emergent geometry and horizon. To see the emergent geometry, we first consider $B_i = \frac{\Delta K_i}{L} = 0$ for simplicity. The transition layer Hamiltonian (5) reduces to Eq. (1) with $e_0^x = -\alpha_x(z)$, $e_0^z = -\alpha_z(z)$, $e_0^y = 0$ and $e_j^i = \delta_j^i$. Thus, $v^i = -\alpha_i(z)$ and $|\mathbf{v}| = |\alpha(z)| = \sqrt{\alpha_x^2 + \alpha_z^2}$. The effective geometry in the transition layer is described by the line element of the induced metric [18]

$$ds^2 = g^{\mu\nu} dx_\mu dx_\nu = -(1 - |\mathbf{v}(z)|^2)dt^2 - 2\mathbf{v}(z) \cdot d\mathbf{r}dt + (d\mathbf{r})^2. \quad (8)$$

Defining a new time by $d\tau = dt + \frac{\mathbf{v}(z) \cdot d\mathbf{r}}{1 - |\mathbf{v}|^2}$, the line element in the cylinder coordinate with a radius $\rho = \sqrt{x^2 + z^2}$ reads

$$ds^2 = -(1 - |\mathbf{v}|^2)d\tau^2 + \frac{d\rho^2}{1 - |\mathbf{v}|^2} + \rho^2 d\varphi^2 + dy^2. \quad (9)$$

The property of the geometry defined by the metric (9) is dependent on the sign of $\alpha_\rho = \alpha \cdot \rho / \rho$. For $\alpha_\rho > 0$ ($\alpha_\rho < 0$), the geometry is black (white) hole-like [18]. The event horizon is determined by $|\mathbf{v}(z)| = |\alpha(z)| = 1$ which is exactly at the critical surface with $z = z_h$. For illustration, we show the spectra and light cones with $\alpha_z(z) = 0$ in Fig. 1 (b) and (c).

Normally, for an isotropic metric, the surface gravity at the event horizon is defined by the normal derivative

of the velocity component normal to the horizon. Here it is $\eta_z = \frac{\partial v_z(z)}{\partial z}|_{z=z_h} = -\frac{\Delta\alpha_z}{L}$. For WSMs, it is often the case that $\Delta\alpha_z = 0$ and then $\eta_z = 0$. Because the non-zero value of the tangent vector $v_x(z)$ breaks the isotropy at the horizon, we can define a columnar surface gravity, which may characterize more interesting behaviors of the transition layer. This is defined by

$$\eta_\rho = \left(\frac{\partial |\mathbf{v}(z)|}{\partial z} \right)_{z=z_h} = \Delta\boldsymbol{\alpha} \cdot \boldsymbol{\alpha}(z_h) \frac{v_F}{L} \quad (10)$$

The Hawking temperature of this emergent black hole horizon is defined by

$$T_H = \frac{\hbar\eta_\rho}{2\pi k_B} = \frac{\Delta\boldsymbol{\alpha} \cdot \boldsymbol{\alpha}(z_h)\hbar v_F}{2L\pi k_B}. \quad (11)$$

The typical value of the Fermi velocity for WSM is $v_F \sim 10^6$ m/s. If the thickness of the transition layer $L \lesssim 10$ nm, $T_H \gtrsim 10^2 \Delta\boldsymbol{\alpha} \cdot \boldsymbol{\alpha}(z_h)$ K. If $\Delta\boldsymbol{\alpha} \cdot \boldsymbol{\alpha}(z_h) \sim 0.1$, the Hawking temperature may arrive at several tens of Kelvin which are experimentally reachable. In principle, a Hawking evaporation may be observed by a thermal spectrum of the transition layer fermion when the layer are forming [19, 41]. Similar to the transsonic wave in the bosonic fluid [8, 42], we have a fermion shock wave with a velocity $\mathbf{v}(z)$. If we consider $\alpha_x(z) > \alpha_z(z)$, e.g., taking $\alpha_z(z) = 0$, we can detect this shock wave along the x -direction.

Chaotic transition layer. To show the chaos, we return to $0 < \Delta K_i \ll K_0$. From the effective theory perspective, we try to solve the Dirac equation

$$H(z)\psi(z, t) = i\partial_t\psi(t), \quad (12)$$

where $H(z)$ is given by Eq. (5) and $\psi^T = (\chi, \zeta)$ is a two-component spinor. The spectrum is no longer as simple as Eq. (2). χ and ζ are coupled in Eq. (12) and we solve $\zeta = \zeta[\chi(z)]$. Without loss of generality, we take $q_x = q_y = 0$. Because $\boldsymbol{\alpha}(z)$ slowly varies, we neglect $\partial_z\boldsymbol{\alpha}(z)$ term in $\zeta[\chi(z)]$. Then, the dominant part of χ 's equation in the large \tilde{z} limit reads

$$\partial_{\tilde{t}}^2\chi - \partial_{\tilde{z}}^2\chi + \omega^2\tilde{z}^2\chi + \dots = 0, \quad (13)$$

where $\tilde{z} = \frac{z}{\sqrt{1-\alpha_z^2}}$ and $\omega = \sqrt{(1-\boldsymbol{\alpha}^2)B_x^2 + (1-\alpha_z^2)B_y^2}$ (See Sec. A of [40] for “...” terms in more details). When $\omega^2 > 0$, Eq. (13) coincides with the Landau levels of a Weyl fermion. When $z > z_h$, outside of the horizon, it happens.

When $|\boldsymbol{\alpha}| > 1$ and $|\alpha_z < 1|$ [43], i.e., inside the horizon, it is possible that $\omega^2 < 0$ after $z < z_c$, a characteristic plane with $z_c \leq z_h$ ($z_c = z_h$ if $B_y = 0$). Eq. (13) becomes

$$\partial_{\tilde{t}}^2\chi - \partial_{\tilde{z}}^2\chi - \lambda_L^2\tilde{z}^2\chi + \dots = 0, \quad (14)$$

where $\lambda_L^2 = (\boldsymbol{\alpha}^2 - 1)B_x^2 + (\alpha_z^2 - 1)B_y^2 > 0$. λ_L is also almost a constant and can be thought as the Lyapunov exponent. Eq. (13) describes an inverted oscillator [35].

This is an intrinsic quantum open system because there is no a normalizable solution if the system is fixed at a finite interval [36]. Coupling to the environment, say the y -direction and the bulk states, the transition layer state inside the characteristic plane $z = z_c$ is quantum chaotic [25, 44, 45].

Lattice model. In order to confirm the quantum chaotic behavior in the transition layer, we study a lattice model on a cubic lattice with a lattice spacing $a = 1$. The periodic boundary conditions in the x - y plane are implicated while the thickness in the z -direction is finite. We label the sizes of type-I/II WSMs and the transition layer as $L_{I/II}$ and L , respectively. We consider minimal models describing the type-I/II WSMs on a periodic cubic lattice with Hamiltonian $H_{I/II}^l$ [46]

$$H_{I/II}^l = d_{I/II,\mu}\sigma^\mu, \quad (15)$$

where

$$\begin{aligned} d_{I/II,x} &= 2\tilde{t}(\cos k_x - \cos K_x^{I/II}) + 2\tilde{t}(1 - \cos(k_y - K_y^{I/II})) \\ &\quad + \frac{\tilde{t}}{2}(\cos 3k_x - \cos 3K_x^{I/II}) + 2\tilde{t}\gamma(1 - \cos k_z), \\ d_{I/II,y} &= 2\tilde{t}\sin(k_y - K_y^{I/II}), d_{I/II,z} = -2\tilde{t}\gamma\sin k_z, \\ d_{I,0} &= 0, d_{II,0} = -2\eta_{II}(\cos k_x - \cos K_x^{II}). \end{aligned} \quad (16)$$

Here \tilde{t} is the hopping strength. We introduce γ , which is a z -dependent parameter (see Eq. (17)), to fine tune the hopping strength in the z -direction. The Weyl nodes are located at $\mathbf{K}^{I/II} = (K_x^{I/II}, K_y^{I/II}, 0)$. The lattice Hamiltonian we use here is given by

$$H^l = \begin{cases} H_{II}^l, & \gamma = \gamma_{II}, \text{ for } n_z \leq L_{II}, \\ H_{II}^l + \xi(H_I^l - H_{II}^l), & \gamma = \gamma_{TL}, \text{ for } L_{II} < n_z \leq L + L_{II}, \\ H_I^l, & \gamma = \gamma_I, \text{ for } n_z > L + L_{II}, \end{cases} \quad (17)$$

where n_z is the lattice site index in the z -direction and $\xi = \frac{n_z - L_{II}}{L}$. In the long wave length limit, the Hamiltonian in the transition layer reduces to the form of Eq. (4) up to a z -dependent function which leads to a line of Weyl nodes (see Sec. C in [40]).

Taking $\mathbf{K}^I = (0.54\pi, 0.46\pi, 0)$, $\mathbf{K}^{II} = (0.5\pi, 0, 0)$, $\eta_{II} = 0.8\tilde{t}$ and considering a half filling lattice with $L = L_I = L_{II} = 100$, we sketch the Fermi arcs and pockets projected to the k_x - k_y plane, the colored regions in Fig. 2. There are the Fermi arcs on the surfaces of WSMs and the Fermi pockets in the type-II WSM as expected. In the transition layer, there are Fermi arcs that connect the type-I Weyl nodes' images and the type-II Fermi Weyl ones with the same chirality. The Weyl nodes' lines slightly deviate from these Fermi arcs and the horizon is at $\xi_h \approx 0.18$ (see Sec. C in [40]). According to the band structures of the lattice model (see Sec. B in [40]), there is no Fermi pocket in the transition layer for $\gamma_I = \gamma_{II} = \gamma_{TL} = 1$ (Fig. 2(a)) while Fermi pockets emerge in the transition layer for $\gamma_I = \gamma_{II} = 1$ and $\gamma_{TL} = 0.7$ (Fig. 2(b)). Detailed information of typical zero energy wave functions in Fig. 2 are presented in Sec.

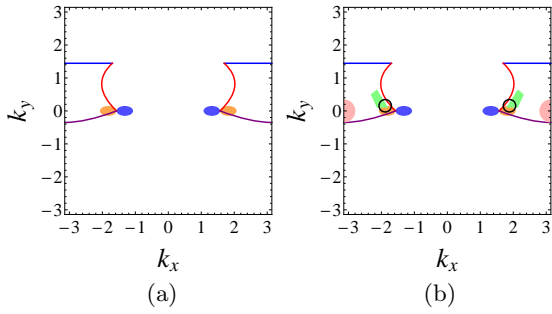


FIG. 2: (color online) The zero energy Fermi arcs and pockets in the k_x - k_y plane. (a) $\gamma_I = \gamma_{II} = \gamma_{TL} = 1$. (b) $\gamma_I = \gamma_{II} = 1$ and $\gamma_{TL} = 0.7$. The spatial distributions of the wave packets are shown in Sec. D of [40]. The blue(purple) Fermi arcs are located on the top(bottom) surface of the type-I(II) WSM. The red Fermi arcs lie in the transition layer and connect to the Weyl nodes's images of the WSMs. The orange and blue regions correspond to the quasiparticle and quasihole Fermi pockets in the type-II WSM. The additional areas in (b) are the pink quasiparticle pockets belonging to the interval inside the horizon in the transition layer, and the green quasiparticle pockets are very close to the horizon from the type-II WSM side. For the meaning of the black circle, see the text.

D of [40], including shapes and spatial distribution of the wave packets, and other numerical data.

OTOCs. The quantum chaos could be measured by OTOCs [1]. We consider the simplest OTOC between the position and momentum operators in the z -direction [37]. In the semiclassical limit, this OTOC describes the dependence on the initial condition of the particle motion. On the lattice, these operators, e.g., are n_z and the difference operator \hat{P}_z which acts on a state $|\psi_{\mathbf{k}}(n_z)\rangle$ where $\mathbf{k} = (k_x, k_y)$ as $\hat{P}_z|\psi_{\mathbf{k}}(n_z)\rangle = \frac{1}{2}(|\psi_{\mathbf{k}}(n_z - 1)\rangle - |\psi_{\mathbf{k}}(n_z + 1)\rangle)$. Here we consider only quasiparticle $|n\rangle = |n_{\mathbf{k}_F}\rangle$ with excitation energy $E_n(\mathbf{k}_F)$ and quasihole $|m\rangle = |m_{\mathbf{k}_F}\rangle$ with excitation energy $E_m(\mathbf{k}_F)$ near the zero energy with a Fermi vector \mathbf{k}_F . Their \mathbf{k}_F -dependent OTOCs are defined by

$$C_T(t, \mathbf{k}_F) = \sum_n \sum_m \frac{1}{e^{\beta E_n(\mathbf{k}_F)} + 1} \left(1 - \frac{1}{e^{\beta E_m(\mathbf{k}_F)} + 1}\right) \times \langle n|[n_z(t), \hat{P}_z(0)]|m\rangle \langle m|[n_z(t), \hat{P}_z(0)]|n\rangle, \quad (18)$$

where $n_z(t)$ and $\hat{P}_z(t)$ are the time-dependent operators in Heisenberg's picture. The \mathbf{k}_F -distribution is given by Fig. 2 and we know which region in the real space the quasiparticle-quasihole pair with a given \mathbf{k}_F comes from in terms of the zero energy states with a given \mathbf{k}_F . For example, if \mathbf{k}_F is on the blue Fermi arcs in Fig. 2(b), the particle-hole pair is from the surface of the type-I WSM while it comes from the inside of the horizon in the transition layer if \mathbf{k}_F is in the pink Fermi pockets. Several OTOCs of typical points of \mathbf{k}_F are plotted in Sec. D of [40]. The measurable OTOCs are the average of these \mathbf{k}_F -dependent OTOCs over a given region \mathcal{A} in

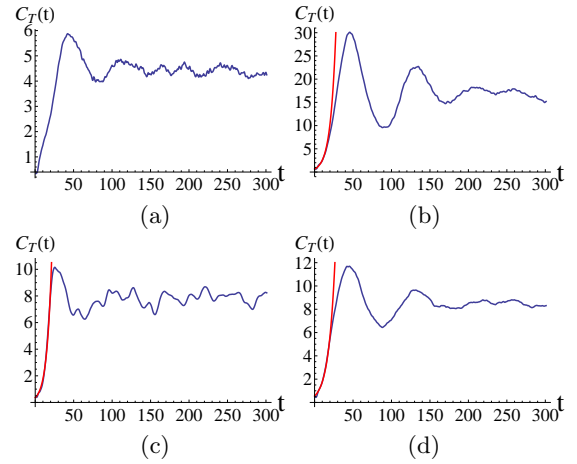


FIG. 3: (color online) The OTOCs $C_{T,\mathcal{A}}(t)$. (a) \mathcal{A} =blue arcs in Fig. 2; (b) \mathcal{A} =blue pockets; (c) \mathcal{A} =pink pockets; (d) \mathcal{A} covers all colored regions in Fig. 2. The red curves are the exponent fitting with the quantum Lyapunov exponents.

Fig. 2

$$C_{T,\mathcal{A}}(t) = \frac{1}{N_{\mathcal{A}}} \sum_{\mathbf{k}_F \in \mathcal{A}} C_T(t, \mathbf{k}_F), \quad (19)$$

where $N_{\mathcal{A}}$ is the number of \mathbf{k}_F in \mathcal{A} .

In numerical calculations, we take $T = 1/\beta = \tilde{t}/30$ and truncate the state summation to twenty lowest energy quasiparticle and quasihole states. For the model with $\gamma_I = \gamma_{II} = 1$ and $\gamma_{TL} = 0.7$, when \mathcal{A} is the blue Fermi arcs (BA) or purple Fermi arcs (PA) in Fig.2(b), which is on the surface of WSM, no fast exponential scrambling is detected. For example, $C_{T,BA}(t)$ is shown in Fig. 3(a) and the scrambling is approximately linear. When \mathcal{A} =the black circle (BC) in Fig. 2(b), $C_{T,BC}(t)$ shows a clear fast scrambling within a short time and then slowly fluctuates along a saturated value (See Fig. 3(b)). The quantum chaos signal is seen with a quantum Lyapunov exponent $\lambda_{QL} = 0.0699$ according to an exponential fitting $\sim e^{2\lambda_{QL}t}$. In the long wave length limit, the lattice Hamiltonian in this region is basically of the form of the effective Hamiltonian (4). The chaotic states spread to inside of the horizon, including both the bulk of type-II WSM and the transition layer (See Sec. C in [40]). The Ehrenfest time T_E , after which the wave function spreads over the whole black/white hole, can be read out: The OTOC saturates after $T_E \approx 170$ -180 $\lesssim L + L_{II} = 200$ instead of growing everlastingly in the classical chaos. This shows a possible distinction between the quantum chaos and the classical one [38]. Furthermore, for the pink pocket (PP) in Fig. 2(b), as seen in Fig. 3(c), $C_{T,PP}(t)$ gives another quantum chaos signal with $\lambda_{QL} = 0.0797$. This quantum chaos does not have an effective model explanation. The corresponding chaotic states are confined within the transition layer inside the horizon, instead of spreading into the bulk of type-II WSM (See C in [40]). The corresponding Ehrenfest time is reduced to

$T_E \approx 70 < L = 100$. The OTOCs for the other regions in Fig. 2 do not give clear chaos signals (See C in [40]). Fig. 3(d) is the OTOC after averaging over all zero energy states in Fig. 2. The fast scrambling is still seen with $\lambda_{QL} = 0.0583$ and $T_E \approx 150$.

For the model with $\gamma_I = \gamma_{II} = \gamma_{TL} = 1$, no fast scrambling appears in Eq. (18) for any given \mathbf{k}_F in Fig. 2(a) due to the lacking of the black circle or the pink regions zero energy states. However, the high energy quantum chaos may exist but this is not the goal for us to probe in this work.

We have seen that the appearance of the fast scrambling is dependent on the hopping strength in the transition layer. Another parameter that affects the fast scrambling is the thickness L of the transition layer. As L decreases, the chaoticity of the quantum states inside the horizon is reduced (see Sec. E in [40]) and so is λ_{QL} [47].

Conclusions. We pointed out that there are emergent black/white event horizons in the transition layer between type-I and type-II WSMS. We found a novel surface gravity on the event horizon and the corresponding Hawking temperature may be measurable. When the Weyl nodes of type-I and type-II mismatch, the quasiparticles moving inside the horizon may be quantum chaotic. We confirm this quantum chaotic behavior in a lattice model by calculating the OTOCs of the system. Two diagnostic quantities, the quantum Lyapunov exponent and the Ehrenfest time, which characterize the quantum chaos, were determined.

This work is supported by NNSF of China with No. 11474061 (YGC,XL,YY) and No. 11804223 (XL) and the ministry of science and technology of China with the grant No.2016YFA0301001 (FYL,GC).

-
- [1] J. Maldacena, S. H. Shenker and D. Stanford, JHEP 1608, 106 (2016).
- [2] A. Kitaev, <http://online.kitp.ucsb.edu/online/joint98/kitaev/>
- [3] A. Kitaev, <http://online.kitp.ucsb.edu/online/entangled15/kitaev/> <http://online.kitp.ucsb.edu/online/entangled15/kitaev2/>
- [4] J. Maldacena and D. Stanford, Phys. Rev. D **94**, 106002 (2016).
- [5] S. Sachdev, Phys. Rev. Lett. **105**, 151602 (2010).
- [6] S. H. Shenker and D. Stanford, JHEP 1403, 067 (2014).
- [7] S. H. Shenker and D. Stanford, JHEP 1505, 132 (2015).
- [8] W. G. Unruh, Phys. Rev. Lett. **46**, 1351 (1981).
- [9] O. Lahav, A. Itah, A. Blumkin, C. Gordon, S. Rinott, A. Zayats, and J. Steinhauer, Phys. Rev. Lett. **105**, 240401 (2010).
- [10] A. Roldan-Molina, A. S. Nunez, and R. A. Duine, Phys. Rev. Lett. **118**, 061301 (2017).
- [11] P. Horava, Phys. Rev. Lett. **95**, 016405 (2005).
- [12] F. D. M. Haldane, Phys. Rev. Lett. **107**, 116801 (2011).
- [13] R. Z. Qiu, S. P. Kou, Z. X. Hu, X. Wan, and S. Yi, Phys. Rev. A **83**, 063633 (2011).
- [14] K. Yang, Phys. Rev. B **93**, 161302(R) (2016).
- [15] X. Luo, Y.-S. Wu, and Y. Yu, Phys. Rev. D **93**, 125005 (2016).
- [16] G. E. Volovik and M. A. Zubkov, Ann. of Phys. **356**, 255 (2015).
- [17] L. Dong and Q. Niu, Phys. Rev. B **98**, 115162 (2018).
- [18] G. E. Volovik, Pis'ma ZhETF **104**, 660 (2016).
- [19] G. E. Volovik, Physics-Uspekhi **61**, 89 (2018).
- [20] J. Nissinen and G. E. Volovik, JETP Lett. **105**, 447 (2017).
- [21] K. Zhang and G. E. Volovik, J. Low Temp. Phys. **189**, 276 (2017).
- [22] H. Q. Huang, K.-H. Jin, and F. Liu, Phys. Rev. B **98**, 121110(R) (2018).
- [23] S. W. Hawking, Nature **248**, 30 (1974); Commun. Math. Phys. **43**, 199 (1975).
- [24] J. D. Bekenstein, Phys. Rev. D **7**, 2333 (1973).
- [25] K. Hashimoto and N. Tanahashi, Phys. Rev. D **95**, 024007 (2017).
- [26] H. B. Nielsen and M. Ninomiya, Nucl. Phys. B **185**, 20 (1981). Nucl. Phys. B **193**, 173 (1981). Phys. Lett. B **130**, 389 (1983).
- [27] F.-Y. Li, X. Luo, X. Dai, Y. Yu, F. Zhang, and G. Chen, Phys. Rev. B **94**, 121105(R) (2016).
- [28] X. Wan, A. M. Turner, A. Vishwanath, and S. Y. Savrasov, Phys. Rev. B **83**, 205101 (2011).
- [29] H. M. Weng, C. Fang, Z. Fang, B. A. Bernevig, and X. Dai, Phys. Rev. X **5**, 011029 (2015).
- [30] S.-M. Huang, S.-Y. Xu, I. Belopolski, C.-C. Lee, G. Q. Chang, B. K. Wang, N. Alidoust, G. Bian, M. Neupane, C. L. Zhang, S. Jia, A. Bansil, H. Lin and M. Z. Hasan, Nat. Commun. **6**, 8373 (2015).
- [31] S. Y. Xu et al, Science **349**, 613 (2015).
- [32] B. Q. Lv et al, Phys. Rev. X **5**, 031013 (2015).
- [33] L. X. Yang et al, Nat. Phys. **11**, 728 (2015).
- [34] A. A. Soluyanov et al, Nature **527**, 495 (2015).
- [35] G. Barton, Ann. Phys. **166**, 322 (1986).
- [36] C. Yuce, A. Kilic, and A. Coruh, Phys. Scr. **74**, 114 (2006).
- [37] A. I. Larkin and Y. N. Ovchinnikov, JETP **28**, 1200 (1969).
- [38] K. Hashimoto, K. Murata, R. Yoshii, JHEP **10**, 138 (2017).
- [39] S. Tchoumakov, M. Civelli, and M. O. Goerbig, Phys. Rev. B **95**, 125306 (2017).
- [40] See *Supplementary Materials*.
- [41] H. Liu, J. -T. Sun, H. Q. Huang, F. Liu, and S. Meng, arXiv: 1809.00479.
- [42] G. E. Volovik, *The Universe in a Helium Droplet*, Clarendon Press, Oxford (2003).
- [43] We do not discuss the case with $|\alpha_z| > 1$. The horizon is not stable in this case.
- [44] W. H. Zurek and J. P. Paz, Phys. Rev. Lett. **72**, 2508 (1994).
- [45] P. A. Miller and S. Sarkar, Phys. Rev. E **58**, 4217 (1998).
- [46] T. M McCormick, I. Kimchi and N. Trivedi, Phys. Rev. B **95**, 075133 (2017).
- [47] The quantum Lyapunov exponent λ_{QL} is not necessary to be exactly the same as λ_L due to the quantum correction. λ_L in the effective model increases first in L increases and

then decreases for the large L . We have yet to see such a decrease for λ_{QL} .